Higher-order equilibria of temporal soliton molecules in dispersion-managed fibers

A. Hause[*,†] and F. Mitschke[†]
Institut für Physik, Universität Rostock, 18051 Rostock, Germany
(Received 30 September 2013; published 23 December 2013)

Bound states of two or three solitons in dispersion-managed fibers (soliton molecules) were experimentally demonstrated recently. We investigate with a modified perturbation analysis whether the binding mechanism creates a unique stable equilibrium of the relative positions of the solitons in the molecule. Indeed, we find a multitude of equilibrium states, alternatingly stable and unstable. This holds for either case: nearest neighbor solitons having the same or the opposite phase. The number of equilibria are limited by the level of the radiation background. The state with the smallest separation and the highest binding energy ("ground state") always occurs for opposite-phase pulses; the lowest-order state for in-phase pulses is always unstable. Stable long-chain molecules can be built with a mixture of different nearest-neighbor equilibrium separations. Our results agree with our numerical simulations and experimental results, and connect well with certain results in the literature.

DOI: 10.1103/PhysRevA.88.063843 PACS number(s): 42.81.Dp, 42.65.Sf

I. INTRODUCTION

Internet traffic is driven by data-hungry novel applications, and its volume increases incessantly. Soliton molecules in dispersion-managed fibers have been suggested as one way to enhance the data-carrying capacity of fibers, possibly in combination with phase and polarization multiplexing [1,2]. This approach is unique in the way it exploits, rather than avoids, the fiber's nonlinearity. It has been recently pointed out [3] that indeed nonlinearity can be used to an advantage in dealing with the Shannon limit [4].

Molecules, i.e., bound states, of solitons are not unique to fiber optics; similar concepts exist in other fields of physics [5–8]. On the other hand, the soliton molecules in dispersion-managed fiber discussed here have a mechanism different from similarly named concepts described in [9–12]. The history of soliton molecules began with the description [13] and first experiment [14] of soliton interaction forces. In 1999, after the introduction of dispersion-managed (DM) fibers, theoretical descriptions of antisymmetric DM soliton molecules (i.e., a pair of solitons in opposite phase, forming a bound state) were presented that used an odd Hermite-Gauss function [15,16]. Maruta *et al*. then published numerical studies of in-phase DM soliton molecules [17] and stable trains of DM solitons [18]. That work was extended in [19] with a higher-order multiscale asymptotic analysis. Similar results were obtained in [16] for solitons in adjacent wavelength channels, and in [20] for fibers with Bragg gratings for dispersion compensation.

A first experimental demonstration was presented in 2005 [21], followed by a report of a full amplitude-and-phase characterization [22] and an explanation of the binding mechanism [23]. Very recently, the concept was extended by the experimental demonstration of three-soliton molecules [1,2]. With four symbols now demonstrated (to wit: no pulse, single soliton, two-soliton molecule, and three-soliton molecule), two bits of information can be coded in a single time step in a soliton format.

This study addresses a question that has arisen for several years now: Do soliton molecules have a unique, single equilibrium separation between the constituent solitons, or can there be several stable states? In the language of molecular physics, one might phrase this as follows: Is there only a ground state or do excited (higher-order) states also exist? The literature provides several hints to the existence of higher-order equilibrium states.

Maruta *et al*. [18] found higher-order equilibrium states in numerical simulations when they determined the asymptotic shape using Nijhof's method [24]. That group then came up with a systematic family tree of stable bound dispersion-managed solitons [25]. Gabitov *et al*. found what they called twin families of bisolitons [26] from an averaged Gabitov-Turitsyn model [27]. Their study of antiphase soliton molecules revealed two branches of solutions, distinguished by their energy; both types can coexist in the DM fiber. In extension of that work, Shkarayev *et al*. [28] revealed the stability properties of the two branches and found a bifurcation point beyond which no molecules exist. In this paper, we endeavor to draw a more complete picture. We use a perturbative treatment similar to that in [23,29], but with a refinement, to calculate interaction forces and equilibrium separations of adjacent solitons. We find conditions under which symmetric in-phase and opposite-phase DM soliton pairs of the same energy can have more than a single equilibrium separation. These equilibria come in stable and unstable types. When the pulse separation is increased, alternating branches of stable and unstable equilibria appear, but the magnitude of the binding energy decreases monotonically. We also locate bifurcation points between the branches representing these equilibria. Moreover, we can make statements regarding long chains of solitons and their interpulse separations.

In Sec. II, the model for the interaction force of adjacent solitons is presented, and an averaging method is used to calculate equilibrium separations with an improved modeling of the pulse wings. It will be shown that consideration of the shape of soliton tails does make a difference. In Sec. III, soliton movements as predicted from the model are compared to numerical simulations. We will show alternating branches of stable and unstable equilibria, and their energy dependence. A possible arrangement of DM solitons at different

[*]alexander.hause2@uni-rostock.de
[†]www.physik.uni-rostock.de/optik

higher-order equilibrium separations in stable soliton trains is also presented. In Sec. IV, we will compare to experimental data.

II. INTERACTION FORCES AND BINDING POTENTIAL

In this paper, we consider only soliton molecules of two or more individual DM solitons with a relative phase of either close to $\varphi = \pi$ or close to $\varphi = 0$. Quite different phases lead to an asymmetric energy transfer between the solitons which may eventually cause the molecule to disintegrate.

A. Propagation equation and soliton characteristics

Optical pulse propagation in constant dispersion fibers is well described by the nonlinear Schrödinger equation (NLSE) with constant parameters β_2 for group velocity dispersion (GVD) and γ for the Kerr nonlinearity. This integrable equation has analytically known solutions; the fundamental soliton has a hyperbolic-secant (sech) amplitude profile which remains invariant during propagation. Its peak power P_0 and temporal width T_0 are connected through the fiber parameters by the constraint $P_0 T_0^2 = \beta_2/\gamma$. Therefore, any of the parameters peak power, width, and energy $E_{\mathrm{sol}} = 2P_0T_0$ can be set as desired when the others are scaled accordingly. The interaction of such fundamental solitons was formulated in [13]. In a more recent and extended version [9], interacting soliton pairs were called "soliton molecules;" however, they do not have an equilibrium separation and must not be confused with the soliton molecules in dispersion-managed fibers treated here.

Let the pulse amplitude profile be represented by $u(t,z)$ with z position and t time in a comoving frame. For the purpose of this study, we do not include in the NLSE higher-order corrections to the dispersion or nonlinearity. The position dependence of fiber parameters $\beta_2(z)$ and $\gamma(z)$ renders the equation into a dispersion-managed version of the NLSE, called DM-NLSE:

$$\frac{\partial}{\partial z}u = -\frac{i}{2}\beta_2(z)\frac{\partial^2}{\partial t^2}u + i\gamma(z)|u|^2u. \tag{1}$$

Typical DM fibers have piecewise constant parameters which alternate periodically. Fiber segments have lengths $L^{\pm}$, where index $+$ $(-)$ is for the normal (anomalous) dispersion segment, respectively. The corresponding dispersion values are $\beta_2^{\pm}$. The dispersion period is $L = L^+ + L^-$; the path average dispersion is $\overline{\beta}_2 = (L^+\beta_2^+ + L^-\beta_2^-)/L$. Usually, a DM fiber line begins with a half segment of anomalously dispersive fiber, followed by a full segment of normally dispersive fiber; then, another half segment of anomalously dispersive fiber concludes the first period. A soliton that propagates in such fiber will experience a change of all its parameters as it traverses one dispersion period. Even though Eq. (1) has no loss term, in the dispersion structure some radiation arises and constitutes a power loss of the soliton. We will neglect this loss and use the approximation that the propagation is lossless. Then, the midpoints of the fiber segments are chirp-free points provided a chirp-free pulse is launched in the first place [30], and the pulse shape will return exactly to its initial shape after one dispersion period, and oscillate periodically thereafter.

The amount of breathing of the DM soliton has been described by the concept of map strength. Several slightly different definitions exist [31–34]: we adopt the form used in [21,35] and implicitly in [36] which is

$$S' = \frac{|\beta_2^- - \overline{\beta}_2|L^- + |\beta_2^+ - \overline{\beta}_2|L^+}{\tau^2}. \tag{2}$$

Here, the pulse width τ is taken at the chirp-free points of the anomalously dispersive segment where it takes its minimum. $\tau = aT_0$ denotes the full width at half maximum pulse width where the numerical factor is $a = \cosh^{-1}(3)$ for sech-shaped pulses, and $a = 2\sqrt{\ln 2}$ for Gaussian pulses. It is an inconvenience that there is no analytic form for the pulse shape; while the fundamental soliton has a sech shape, neither sech nor Gaussian describe a DM soliton accurately. Note that a variation of the soliton energy leads, by way of scaling of the pulse duration, to a change in S' even in the same fiber.

A more detailed characterization of the parameter alternation was introduced in [18,25]. The (B, S, R) triplet includes the accumulated dispersion $B = (\beta_2^- L^- + \beta_2^+ L^+)/\tau^2$, the map strength (defined slightly differently from above) $S = (-\beta_2^- L^- + \beta_2^+ L^+)/\tau^2$, and a metric of the nonlinearity allocation $R = \gamma^- L^-/(\gamma^- L^- + \gamma^+ L^+)$.

In the absence of an analytic pulse shape, one wishes to obtain the shape numerically with the best possible precision. This can be accomplished, e.g., by Nijhof's iterative method [24]. One should note that even the most precise approximation only yields a shape which still suffers radiative losses in the long haul which we neglect here.

Generally, DM solitons near the chirp-free points tend to have Gaussian character near their center (in particular for large S'), whereas away from the center eventually sech-like wings appear. The wings may have an oscillation on top of their general shape [37–41]. Away from the chirp-free points, and in particular near the segment splices where the pulse width takes its maximum, oscillations in the tails tend to disappear.

A Gaussian ansatz as an approximation to a DM soliton shape captures the central part quite well and is therefore almost universally adopted (e.g., [42,43]); it is a reasonable ansatz to describe the ground state of soliton molecules [23,29]. It meets its limitations, however, when details of the wings count: The tails of Gaussian, sech, and "true-soliton" pulses are quite different, and any conclusions about higher-order equilibria or interactions between adjacent solitons are affected considerably.

B. Averaging method

We now describe our semianalytical method to find equilibrium separations of DM solitons. Consider a soliton with complex amplitude profile $u_0(t,z)$ which is in interaction with some other solitons $u_1, \ldots, u_n$ close to it. Their individual energies are $E_{\mathrm{sol},j} = \int_{-\infty}^{\infty} |u_j|^2 dt$. We use the assumption that all solitons have the same shape $u_j(t,z)$ and energy E_{sol}, and are equidistant to each other, i.e., have the same nearest-neighbor separation σ. We do, however, allow for phase differences to the previous soliton $\varphi = \varphi_j - \varphi_{j-1}$ which are all equal, and either 0 or π. Then, the soliton shapes can

be written as

$$u_j(t,z,\sigma,\varphi) = u_0(t - j\sigma,z)\exp(ij\varphi). \tag{3}$$

As shown in [23], the interaction creates a local center frequency shift $d\langle\omega\rangle_0/dz$ of the fiducial soliton. This shift will depend on the interaction strength, and thus on σ; it will also vary with z because the soliton shapes u_j vary periodically within the dispersion period. The shift takes the form

$$\Delta\Omega(z,\sigma,\varphi) = \frac{d}{dz}\langle\omega\rangle_0 = -\frac{\gamma(z)}{E_{\rm sol}}\int_{-\infty}^{\infty}|u_0|^2\frac{\partial}{\partial t}\left(\left|\sum_{j=0}^{n}u_j\right|^2\right)dt. \tag{4}$$

In the presence of dispersion, a frequency change translates into a velocity change $\beta_2\Delta\Omega$ which we metaphorically call a force. Velocity here has units of s/m; the force, s/m^2. Integration over one dispersion period L yields the effective force

$$F_{\rm eff}(\sigma,\varphi) = -\frac{\overline{\beta}_2}{L}\int_0^L \Delta\Omega(z,\sigma,\varphi)\,dz. \tag{5}$$

When in a given fiber the relative phase and soliton energy are also given, the effective force depends on the separation as the only parameter. An effective binding potential $V_{\rm eff}$ of the soliton molecules can then be calculated from

$$F_{\rm eff}(\sigma) = -\frac{\partial}{\partial\sigma}V_{\rm eff}(\sigma), \tag{6}$$

which is in units of s^2/m^2. The binding energy is then given by $\Delta V_{\rm eff} = V_{\rm eff}(\infty) - V_{\rm eff}(\sigma_{\rm eq})$.

In order to verify the existence of an equilibrium, in [23] we assumed Gaussian pulse shapes for $u_j(t)$ and used a perturbation ansatz; a single equilibrium position was found. At close separations, that approach becomes inaccurate because the perturbation is no longer small. It is important to note, however, that the same approach does not at all become better for very large separations: The far wings of real DM solitons are not well represented by Gaussians. One might try to use sech shapes as a more appropriate approximation, but it turns out that that still does not capture the phase dynamics which is important here. Therefore, we here use numerically found shapes of the respective single DM solitons, obtained from Nijhof's averaging method [24], as an even better approximation. This, indeed, provides fresh insights.

Specifically, we run numerical propagations over a complete dispersion period L to obtain the complex amplitude profiles at each position z. From that, the local and effective forces and the molecular potentials are calculated for the two-soliton molecule as well as the three-soliton molecule. In Fig. 1, the molecular potentials are plotted for $\varphi = \pi$ and for energy values of $E_{\rm sol} = 3\ldots15$ pJ. Particulars of the DM fiber are as in the experiments of [1,2], and are detailed in Table I in the Appendix. We refer to this fiber system as Ⓐ, to distinguish from a different fiber below.

For all calculations, the fiducial soliton ($j = 0$) is the leading soliton in the molecule. In that case, minima of the potential curves define stable equilibrium separations $\sigma_{\rm eq}$ (black points in Fig. 1). One can clearly see that with increasing

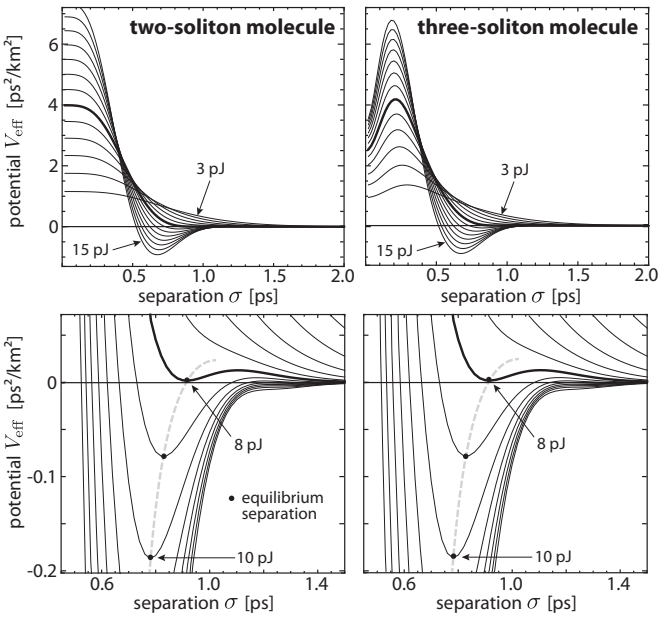

FIG. 1. Binding potential of opposite-phase two-soliton molecules (left) and three-soliton molecules (right) for DM fiber system Ⓐ. Energy is varied from 3 to 15 pJ in 1-pJ increments. Bottom panels: magnified view; equilibrium points are marked by black dots. Note the small potential barrier in some of the curves.

soliton energy the potential minimum gets deeper and moves to smaller separation, i.e., the bond becomes tighter and stronger. Below a certain energy value (here ≈7.5 pJ), no local minimum exists. Note that by definition the potential tends to zero for infinite separation, but for energies around 8 pJ there is a small potential barrier. The depth of the potential well (binding energy) is therefore not identical to the energy required to separate the molecule (dissociation energy); in a very narrow energy range between 7.5 and 8 pJ (not explicitly shown), the equilibrium is even metastable. The equilibrium separations of the two-soliton and three-soliton compounds are nearly the same.

Calculations of the effective force are time consuming because the integrals of the local force Eq. (4) need to be solved numerically for each value of σ and z. The following simplification speeds the process considerably: Averaging of the complex amplitude profile yields an average pulse profile $\overline{u}_0$. Considering the phase profile $\phi_{\rm sol}(t,z)$ of the fiducial soliton, we note that a chirp naturally arises due to the high local dispersion. This chirp evolves from zero at a midpoint of an anomalously dispersive segment until the midpoint of the normally dispersive segment (the other chirp-free point), then evolves back in the same manner. It therefore suffices to extend the integral in Eq. (7) over one half of the dispersion period:

$$\overline{u}_0(t) = \frac{2}{L}\int_0^{L/2} u_0(t,z)\,\exp[-i\phi_{\rm sol}(t=0,z)]dz. \tag{7}$$

With the use of $\overline{u}_0(t)$ an approximate value of the effective force can be obtained directly from Eq. (4). This is shown in Fig. 2 for several energy values (dashed lines) along with corresponding results of the full calculation (solid). Again, the

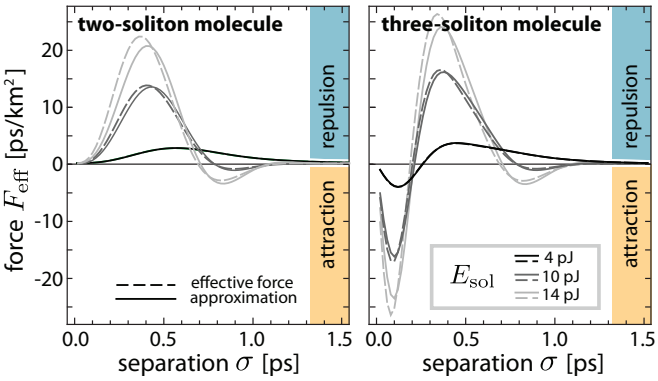

FIG. 2. (Color online) Effective force acting on the fiducial soliton u_0 in an opposite-phase soliton molecule in DM fiber system Ⓐ. Left: two-soliton molecule; right: three-soliton molecule. Solid curves: approximate solution from Eq. (7); dashed curves: full calculation.

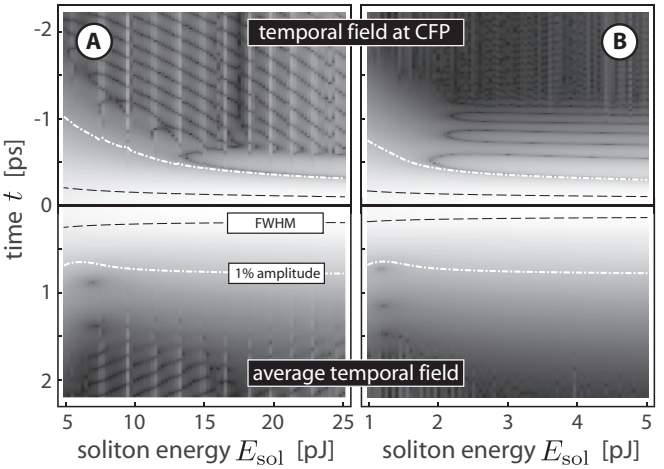

FIG. 3. Pulse profiles of DM solitons are displayed in grayscale; dependence on soliton energy $E_{\rm sol}$ is shown. Left panel: amplitude profiles in DM fiber system Ⓐ; right panel: amplitude profiles in DM fiber system Ⓑ. Upper half: pulse shape at the chirp-free points (CFP) in the anomalous fiber segment. Lower half: average DM soliton shape. Black dashed lines mark the contour at the half width τ, and white dashed-dotted lines that at 1% amplitude.

left panel shows the two-soliton case, and the right panel, the three-soliton case. In all cases, negative frequency shifts of the leading soliton correspond to an equal positive shift of the trailing soliton. At anomalous average dispersion of the DM fiber, this corresponds to a mutual attraction of the solitons. Reversed signs correspond to a repulsion.

As Fig. 2 shows, the results from the approximation (7) agree acceptably well with the full calculation: in the low-energy limit they are nearly identical, and only at high-pulse energies do slight deviations arise. Below, we will therefore use the approximation throughout.

For large separations, the interaction is diminished. It is therefore not surprising that above $\sigma \approx 0.5$ ps, two- and three-soliton cases hardly differ. For narrow separations there are differences, however. There is only repulsion for the two-soliton molecule, whereas for the three-soliton molecule a regime of attraction exists. Apparently, the attraction between the in-phase "outside" pulses overcompensates the repulsion of each with the central opposite-phase pulse.

III. HIGHER-ORDER EQUILIBRIA

The situation may arise that in an n-soliton molecule an equilibrium separation (vanishing net force) between two solitons does not have a single, unique value but several. In such cases, we call an arrangement at the smallest σ value the "ground state," the others, "higher-order states."

A. Effective force in different fiber systems

Stable higher-order states of DM solitons have already been found numerically in [18] in a parameter range of $(B,S,R) = (-0.1,2.3,0.8)$. For ease of comparison, we introduce here a second DM fiber system (system Ⓑ) which closely matches these parameters when $E_{\rm sol} = 2.2$ pJ. Fiber parameters are given in Table II in the Appendix. For comparison, the pulse profiles of both DM fiber systems considered here are shown in Fig. 3 on a logarithmic grayscale, for a range of pulse energies. Energy is varied on the abscissa; all profiles were obtained with Nijhof's method. In the upper half, profiles are shown at the chirp-free point of the anomalous fiber segment; in the lower half, average profiles are shown. Black dashed lines mark the contour at the full width at half maximum, and white dashed-dotted lines that at 1% of maximum.

The data show that the width at the chirp-free point decreases with increasing energy. The amount of overlap of adjacent pulses is better represented by the average shape, though, and that has an opposite trend in its far wing as is best seen at the 1% contour.

Interestingly, at the chirp-free point and above a certain minimum energy (≈13 pJ for Ⓐ, ≈2 pJ for Ⓑ) structures in Fig. 3 appear which look like horizontal, stretched horseshoes. They represent oscillating tails in the pulse shape as described in [37–41]. In the averaged profiles they disappear, and therefore are not of primary relevance for higher-order states. Note that in Ⓐ only the first "horseshoe" is visible. This is explained by different levels of radiative background. Fiber Ⓐ was inspired by an experiment in which dynamics was to be studied in a finite total length; hence, $\bar{\beta}_2$ was chosen relatively large in relation to the local dispersion values, whereas it is much smaller in Ⓑ. As a consequence, the background level is much higher in Ⓐ and swamps the far wings. Where the power has fallen to background level, for fiber Ⓐ a line pattern appears. It might be mistaken for hatching inserted for highlighting which it is not; the reason will become apparent from Fig. 4.

The upper part of Fig. 4 shows power profiles of averaged DM solitons in both systems on a log scale, and clearly reveals the different background levels. In Ⓑ it is at the numerical noise level. In Ⓐ, due to periodic boundary conditions used in the calculation, periodic structure arises in the background which is an otherwise harmless artifact; however, it explains the apparent hatching in Fig. 3.

The lower part of Fig. 4 shows calculations of the effective force for either fiber system; for each we distinguish $\varphi = 0$ (dashed lines) and $\varphi = \pi$ (solid lines). Equilibria (vanishing net force) exist at the zeros of these curves; stable equilibria

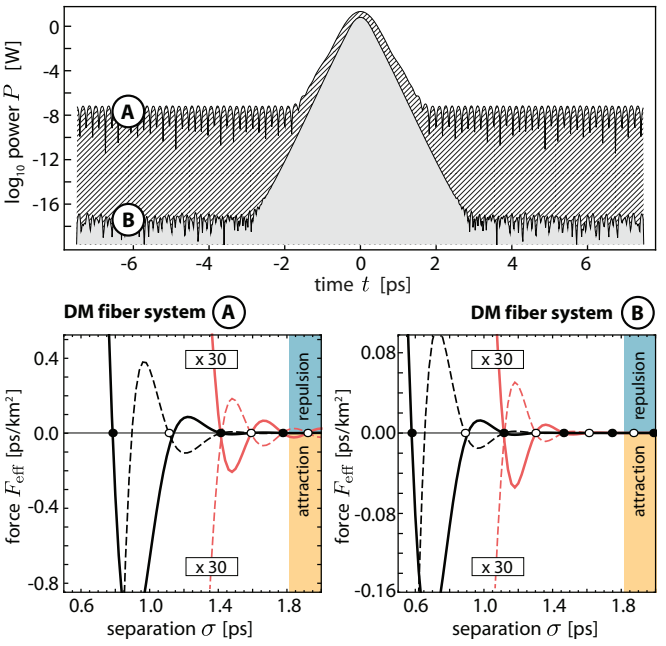

FIG. 4. (Color online) Upper panel: power profiles of average DM solitons in fiber Ⓐ at $E_{\rm sol} = 10$ pJ and Ⓑ at $E_{\rm sol} = 2.2$ pJ. Lower panels: effective force on fiducial soliton u_0 in a two-soliton molecule. Solid curve: $\varphi = \pi$; dashed curve: $\varphi = 0$. Stable equilibria are marked by black (opposite-phase) and white (in-phase) dots.

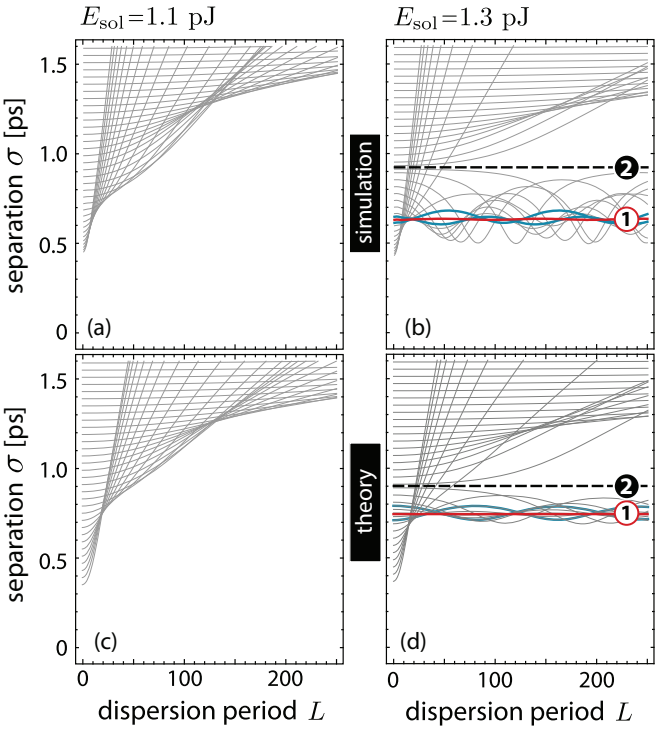

FIG. 5. (Color online) Evolution of the separation σ of an opposite-phase soliton pair in the long haul (250 dispersion periods) when the initial separation σ_0 is varied. (a), (b) Results from a full numerical simulation of the DM-NLSE in fiber system Ⓑ. (a) Single-pulse energy 1.1 pJ; (b) 1.3 pJ. In (a) there is no bound state; in (b) the stable equilibrium is at ①, and an unstable equilibrium at ②. Panels (c), (d) show corresponding results from the simplified model; good agreement is obvious.

are characterized by a negative slope of the effective force so that there is repulsion (attraction) at separations below (above) the zero, respectively. These stable equilibrium positions are marked by black (white) dots for opposite-phase (in-phase) molecules. Intersection points with a positive slope correspond to an unstable equilibrium and are not marked here. The ground state (closest stable separation) occurs for opposite-phase solitons in all cases. As the separation is increased, in-phase and opposite-phase equilibria appear in alternation.

B. Molecule formation and movement of pulses

With interaction forces and molecular potentials derived, we can now fix the initial separation σ_0 and calculate the motion of solitons, in particular, the evolution of $\sigma(z)$ during propagation down the fiber. The latter, calculated for DM fiber system Ⓑ and for opposite-phase pulses, is shown for a range of σ_0 values (initial velocity is zero throughout) in Fig. 5 in the lower half. For comparison, the upper half shows the corresponding full numerical simulations of Eq. (1). Here, we use the full width at half energy, rather than the difference of coordinates of maxima, to obtain the separation $\sigma(z)$ reliably.

In Figs. 5(a) and 5(c), the situation at a single-pulse energy of 1.1 pJ is shown. All trajectories, regardless of σ_0, diverge; this indicates that at this energy a molecule does not exist. This is explained by noting that for low energies, and thus map strengths, the DM soliton shapes approach unchirped sech functions. Opposite-phase standard solitons always experience repulsion; at low energy, only a weak chirp remains and contributes to an attractive force, but not enough to compensate the repulsion. At the slightly higher energy of 1.3 pJ in Figs. 5(b) and 5(d), all trajectories above $\sigma_0 \approx 0.9$ ps (see the line highlighted by the symbol ②) still diverge. Following, for 0.6 ps $\leqslant \sigma_0 \leqslant$ 0.9 ps, they oscillate around the position highlighted by the symbol ①. Further below, trajectories again diverge. Obviously, there is a capture range within which there is a stable equilibrium at ①; such oscillations around the equilibrium are well known [23]. The separatrix at ② marks an unstable equilibrium. For the energies considered here, in-phase soliton pairs are always mutually attracted (not shown).

Figure 5 demonstrates the existence of a ground state and an unstable state. In Fig. 6, we show that several stable and unstable states can exist. The figure combines propagation data over a long distance (250 dispersion periods) on two-soliton molecules (left half) and three-soliton molecules (right half), each for in-phase and opposite-phase pulses (see labels), and also for both full numerical simulation (upper row) and approximate theory (lower row). All data are for DM fiber system Ⓑ at a single-pulse energy of 2.2 pJ. Stable equilibria are identified by circled numbers; unstable equilibria are not specifically marked for the sake of clarity.

In the left half (soliton pair), there is a ground state of the opposite-phase pair (①), but above it there are two more stable states (③ and ⑤). For the in-phase pair, there are also stable states (② and ④) which fall between the former ones in their σ values. The agreement between simulation and theory is obvious.

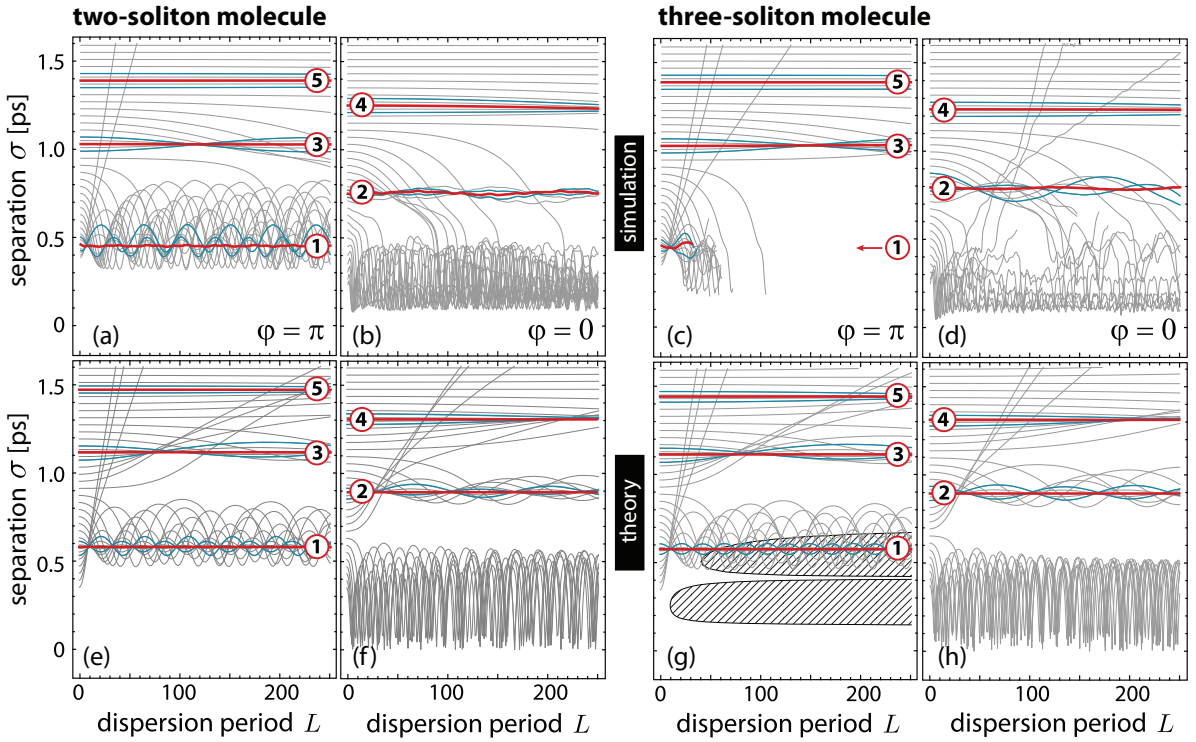

FIG. 6. (Color online) Evolution of the separation of soliton molecules over 250 dispersion periods in dependence on the initial separation σ_0. Data are for fiber system Ⓑ at energy of 2.2 pJ; panels (a), (b), (e), (f) are for soliton pairs, and (c), (d), (g), (h) for triplets. The upper row is from simulation, the lower row from theory. For both types of soliton molecules, up to five stable equilibrium separations with alternating relative phase (starting with $\varphi = \pi$) are found in both theory and simulation. Also, for both types the equilibrium separation values are nearly equal. The ground state of the three-soliton molecule survives only for about 35 dispersion periods (see text).

For pulse triplets, the essential patterns are repeated (right half of Fig. 6). In the simulation, the only major difference is that the ground state (①) decays after ≈35 dispersion periods (still a long distance). In the corresponding theoretical result below, the same does not happen because theory assumes a fixed phase relation and does not capture the cumulative effects of phase shifts during propagation. To assess the limits of validity of the theoretical model, we provide an additional clue: The shapes of two-soliton molecules have perfect symmetry which is unaffected under the action of both Kerr nonlinearity and dispersion. In that context, the only decay mechanism is radiative power loss. In a three-soliton molecule, the power of the center pulse is either enhanced or reduced through interference with the other pulses, depending on the relative phase. Once its power is different from the other pulses, the center pulse has a different rate of phase rotation as it propagates; thus, the phase relation is perturbed. If this continues for a sufficiently long distance, the phase relation may even be reversed, and the triplet is likely to fall apart. As an estimate of the critical distance for this failure, we created a superposition of three averaged DM solitons at the relevant separation. Considering interference effects, the center pulse has a different peak power than the other pulses. From that difference, we calculate the relative phase rotation, and extrapolate to the point where it reaches π. This limit is shown as the line bordering the hatched area; inside that area, the theory can not claim validity. Indeed, the decay as seen in the simulation occurs at a position which is consistent with this argument. For in-phase pulse triplets [Figs. 6(d) and 6(h)] the same interference mechanism, which tends to enhance the center pulse, does not have the same consequences because the equilibrium separations are larger.

Note that opposite-phase pulse triplets can not be constructed for $\sigma_0 < 0.25$ ps because the center pulse disappears altogether; similarly, in-phase pulses at the same close distance merge together immediately. No soliton molecules can then be formed.

The fiber parameters of system B were chosen close to the system of Ref. [18] at the energy level used there; therefore, we can also draw quantitative comparisons between that paper and Fig. 6. Stable equilibria were reported; the lowest occurs at opposite phase; the others alternate between in phase and opposite phase. Separations were given in units of pulse widths τ; we translate our data to the same for ease of comparison. To do so, we find the τ value pertaining to the power used which is $\tau = 259$ fs. Beginning at the ground state, equilibria were located in [18] without any claim of precision at separations of 2τ, 3τ, 4τ, and 5τ, respectively. We find them at 2.22τ, 3.44τ, 4.32τ, and 5.06τ. The agreement, given the difficulty of comparison, is satisfactory.

C. A multitude of equilibrium states

In suitable cases there can be a multitude of stable equilibrium states, alternatingly for opposite-phase and in-phase pulses. To organize this multitude, we investigate the global structure of parameter space, with relevant parameters pulse energy E_{sol} and initial separation σ_0. We concentrate on DM

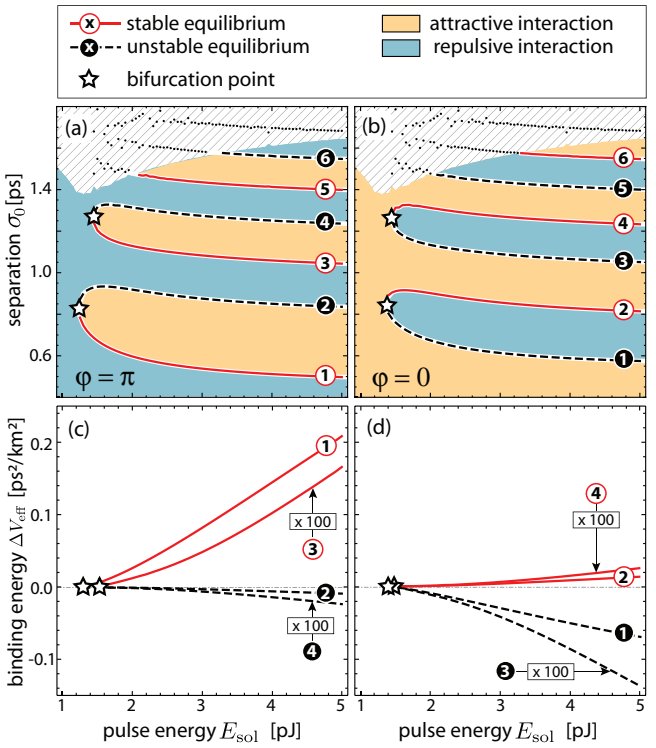

FIG. 7. (Color online) Stability properties of two-soliton molecules in the ($E_{\rm sol}$, σ_0) plane for DM fiber system Ⓑ. Upper panels: equilibrium separations calculated for relative phases of $\varphi = \pi$ (left) and $\varphi = 0$ (right). Stable (unstable) equilibria are marked by solid red (dashed black) curves and circled numbers, respectively. In blue regions, the solitons repel, and in orange regions, they attract. In the hatched regions, equilibria are strongly affected by the radiative background and therefore data become unreliable. Lower panels: binding energy of the equilibria identified by circled numbers; branches appear pairwise at positions highlighted by asterisks. Positive (negative) values correspond to stable (unstable) cases.

fiber system Ⓑ which admits more states; we will return to Ⓐ in the following for a comparison to experiments.

The upper panels of Fig. 7 show data obtained for each energy level. Equilibrium states are characterized by vanishing effective force; if there is attraction for $\sigma_0 > \sigma_{\rm eq}$, the equilibrium is stable. Red solid lines denote stable states, and black dashed lines, unstable states. Areas enclosed by these lines correspond to attractive (yellow) or repulsive (blue) force, respectively. At too large separation, due to radiative background the approximation is no longer trustworthy; the corresponding area is hatched. In the lower panels, the binding energies pertaining to the branches are given in corresponding line styles; for better visibility, the very small values for ③ and ④ are shown magnified as indicated.

As above, we again find that the smallest stable separation (①) occurs for opposite-phase pulses; this would be the first state one expects to find in experiments as it has the strongest bond. The limiting point (saddle-node bifurcation) of the first "tongue" of attraction is marked by an asterisk and indicates the threshold energy to establish a soliton molecule; below threshold the usual repulsion between weakly chirped opposite-phase pulses prevails. Similarly, higher-order states have thresholds, but these are slightly larger. As the lower panels of Fig. 7 show, they also have significantly lower binding energy and are therefore likely to be more vulnerable to perturbations. In-phase soliton pairs always have an unstable ground state.

When one endeavors to create long chains of molecules, one may mitigate the problem of unequal powers by arranging solitons at higher-order equilibrium separations. Figure 8 shows that larger molecules built in this way can propagate stably over very long distances (here, 300 dispersion periods). As an example, Fig. 8(a) demonstrates how soliton molecules of up to five pulses can be built when the second opposite-phase equilibrium separation ③ is used throughout. Figures 8(b) and 8(c) show examples of five-soliton molecules where different pulse separations and different relative phases are mixed. The individual separations used are identified by circled numbers corresponding to the previous figures. For reference, the input shapes are shown (black), the output shapes after a propagation of 300 dispersion periods (gray). Comparison shows that the shape is well maintained.

IV. COMPARISON TO EXPERIMENTAL DATA

In order to compare our results with experimental findings, we now concentrate on DM fiber system Ⓐ. We mapped out

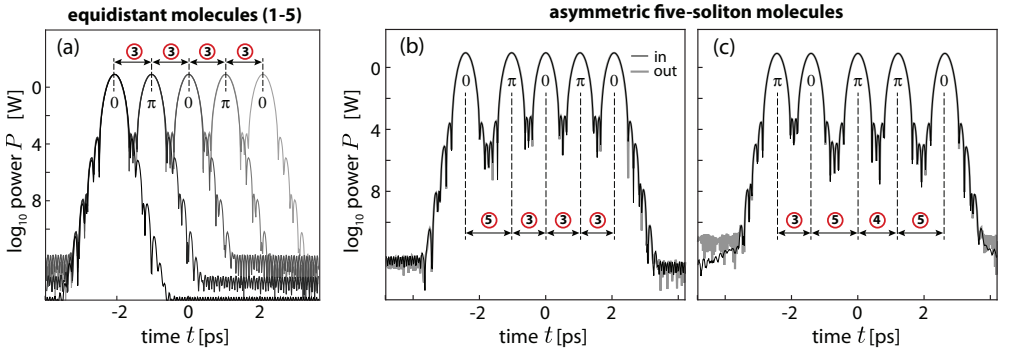

FIG. 8. (Color online) Construction of trains of dispersion-managed solitons. Shown are shapes after numerical propagation and application of Nijhof's method for DM fiber system Ⓑ at pulse energy $E_{\rm sol} = 2.2$ pJ. (a) Starting with a single DM soliton, up to four more solitons can be attached with a separation taken as the second stable location ③. (b), (c) Examples of the propagation of five-soliton molecules over 300 dispersion periods with different intersoliton separations and relative phases. Input shapes, black lines; output shapes, gray lines.

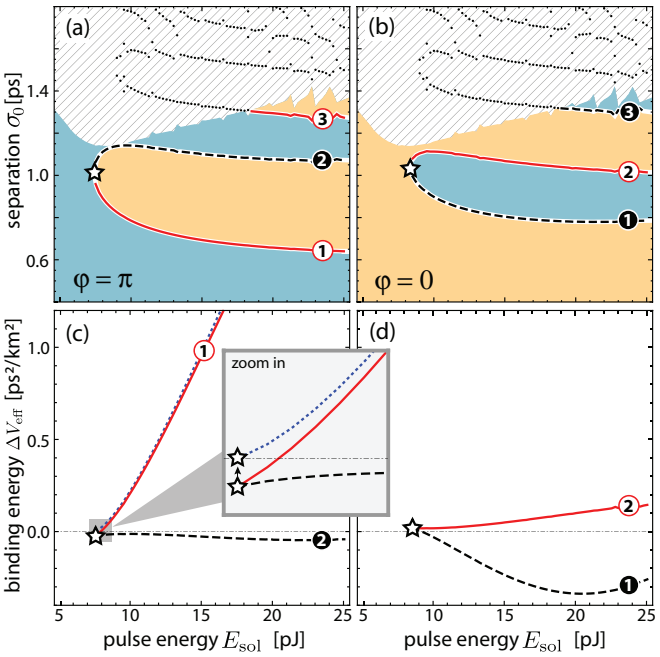

FIG. 9. (Color online) Stability properties of two-soliton molecules in the ($E_{\rm sol}$, σ_0) plane for DM fiber system Ⓐ, otherwise as in Fig. 7. Inset of (c): magnification showing that binding energy (red solid lines) and dissociation energy (blue dotted lines) are not identical (see text).

the stability in the ($E_{\rm sol}$, σ_0) plane in the same way as in Fig. 7; Fig. 9 shows that the situation is qualitatively similar. One distinction is that the binding potential in this case has a noticeable barrier (compare the discussion accompanying Fig. 1 above). Therefore, in the magnification (inset) of Fig. 9(c) we make the distinction between binding and dissociation energy.

A quantitative comparison with experimental data obtained in [2] yields the following: The lowest threshold energy for formation of a stable soliton molecule pertains to an opposite-phase pair. Our model suggests that this is the only stable molecular equilibrium due to relatively strong radiative background; this conclusion is supported by the experiment. According to Fig. 9, the threshold energy is $E_{\rm th} = 7.45$ pJ, in excellent agreement with the experimental observation of $\approx$7 pJ. Using the same soliton energy of $E_{\rm sol} = 11.7$ pJ as in the experiments, the equilibrium separation $\sigma_{\rm eq} = 0.72$ ps matches the experimental value of $\sigma_{\rm eq} = 0.74$ ps quite closely. This can be seen in the upper part of Fig. 10. Data were taken for a range of initial separations (vertical axis); the left panel shows cross-correlation traces, the center panel the separations extracted from the data, and the right panel velocities which were also obtained from the cross-correlation measurements (compare [2]). For reference, the center panel also shows the bisector, i.e., the locus of points where the input separation equals output separation. It is plain to see that the initial separation was maintained at $\sigma_{\rm eq} = 0.74$ ps. As the slope of crossing this point indicates, for smaller initial separations there was repulsion and vice versa; this is the signature of a stable equilibrium. Correspondingly, at the same point, the velocity in the right panel becomes zero.

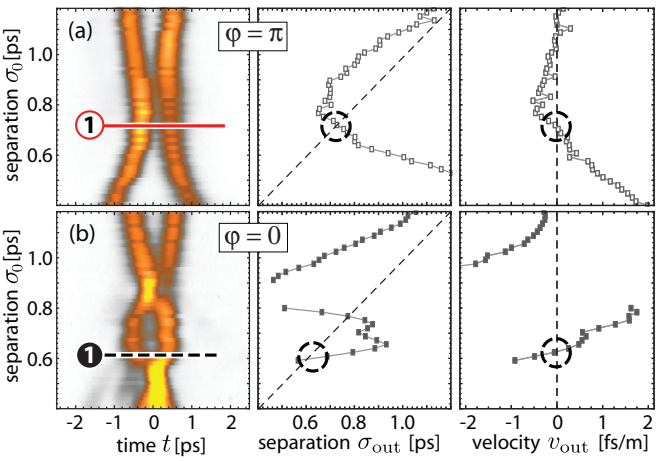

FIG. 10. (Color online) Experimental data to find equilibrium states. Left: cross-correlation data shown in color code from near zero (white) through gray and orange to yellow (highest value) for a range of input pulse separations σ_0. Center: extracted output separation $\sigma_{\rm out}$; note that the bisector is the locus of unchanged separation. Right: relative velocities as obtained from cross-correlation data. Upper row: for the opposite-phase soliton pair, the ground state is located at the highlighted position. Lower row: for the in-phase pair, an unstable equilibrium is revealed at the highlighted position.

The lower part of Fig. 10 shows data taken for in-phase soliton pairs. At the marked position the position is unchanged, but the slope of crossing is reversed, indicating an unstable equilibrium. The velocity is zero again. This is experimental evidence for the existence of the unstable lowest-order state of in-phase soliton molecules, and corroborates our analysis. Unfortunately, the position of the unstable equilibrium does not fit well in quantitative terms with the other data; the reason goes unexplained for now.

V. CONCLUSIONS

We have investigated the binding mechanism of soliton molecules in dispersion-managed fibers. We used a semianalytical model to calculate the binding potential and interaction forces of adjacent solitons; the method is modified over earlier, similar approaches in that we use a realistic shape of the pulse's far wings rather than the coarse approximation of Gaussian shapes previously employed.

We find that the interaction provides the possibility of more than a single separation where all forces balance out. Indeed, there is an entire hierarchy of separations with increasing pulse-to-pulse separation; at the smallest separation, one finds the strongest binding which is then progressively diminished as the separation is increased. This suggests to call the equilibrium positions "ground state" and "higher-order states," respectively.

In the case that adjacent solitons have opposite phase of each other, the ground state is stable; this is the situation that has been described in experiments [1,2,21]. Higher-order states are alternatingly unstable and stable. If adjacent solitons are in phase, the lowest-order state is unstable; beyond, there is the same alternation of stability. The hierarchy of states in the in-phase and opposite-phase states are interleaved in their

separation values. We emphasize that while the existence of a hierarchy of equilibrium separations may suggest that it is caused by the oscillating tails of DM solitons, this can not be so because we use an averaged expression for the tails which is not oscillatory.

The total number of equilibrium states is limited because in the unavoidable presence of radiative background in the fiber, the far wings of the pulses are swamped at some point. This explains why in the reported experiments, in which the background level was relatively high, only the ground state was described; however, here we showed data demonstrating the lowest-order state for in-phase pulses.

The results of our treatment match well with both numerical simulations and experimental data. Both the threshold energy for generation of a ground-state molecule and its separation are predicted in agreement with experimental data. Theoretical approaches attempting to construct soliton molecules from a Gauss-Hermite ansatz [15,16] predict, by logical extension, that longer-chain molecules exist; however, they preclude by ansatz the possibility of different equilibrium separations. We conclude that the Gauss-Hermite approximation does not capture some essential features. On the other hand, the hierarchy of stable states found numerically in [18] is confirmed almost perfectly in a qualitative sense, and even quite well quantitatively. Moreover, the result that molecules can exist on two branches [26,28] is now embedded in a wider picture. We also show that soliton molecules of even more constituent pulses can be constructed when one adheres to the stable separations. Even mixing different orders of equilibrium is possible. This is in many ways similar to the behavior of dark DM solitons that can also be arranged into long chains with several different separations [44].

It is only appropriate that we point out one caveat: In DM fibers, solitons always suffer from radiative loss, and in this sense they neither repeat their shapes periodically nor do they live forever. This does not prevent commercial DM systems from functioning well. Soliton molecules suffer from the same loss mechanism. The opposite-phase three-soliton molecule seems to be particularly affected as both the "outside" pulse interacts destructively with the center pulse. In a similar molecule, but with the next-higher equilibrium, this problem is mitigated. In order to find the molecule of the best long-term stability, one may have to weigh this interference problem against the lower binding energy of the higher-order state.

We may also point out that an apparently similar phenomenon of soliton-pair formation at a set of discrete separations was reported for fiber lasers [45]. However, the similarity, while striking, is superficial: It is a signature of lasers that there is gain to balance the outcoupling loss; in contrast, we study a passive, near-lossless system. This distinction is reflected in the fact that the relevant underlying equation in fiber lasers is the Ginzburg-Landau equation, whereas we deal with the nonlinear Schrödinger equation. As one consequence, soliton pairs in lasers typically appear with a relative phase of $\pi/2$, whereas here we find phases of 0 and π. According to [45], pair separations in fiber lasers are governed by interaction with radiation (Kelly sidebands). In our case, separations are governed by pulse chirp, and radiation is only a minor perturbation to that mechanism.

ACKNOWLEDGMENT

We thank P. Rohrmann for taking the data in Fig. 10. Financial support by Deutsche Forschungsgemeinschaft is gratefully acknowledged.

APPENDIX: FIBER LINE SPECIFICATIONS

Tables I and II present the parameters of DM fiber systems Ⓐ and Ⓑ.

TABLE I. Parameters of DM fiber system Ⓐ which correspond to the fiber used in experiments in [1,2]. τ is obtained from Nijhof's averaging method [24].

$\beta_2^- = -5.16$ ps^2 km^{-1}	$\beta_2^+ = 4.26$ ps^2 km^{-1}
$\gamma^- = 1.72$ W^{-1} km^{-1}	$\gamma^+ = 1.72$ W^{-1} km^{-1}
$L^- = 24.0$ m	$L^+ = 22.0$ m

$\lambda_0 = 1540$ nm
$\overline{\beta}_2 = -0.65$ ps^2 km^{-1}
$\overline{\gamma} = 1.72$ W^{-1} km^{-1}
S'@3 pJ $= 0.710$ ($\tau = 552$ fs)
S'@15 pJ $= 3.038$ ($\tau = 267$ fs)
(B,S,R)@3 pJ $= (-0.099, 0.714, 0.522)$
(B,S,R)@15 pJ $= (-0.423, 3.056, 0.522)$

TABLE II. Parameters of DM fiber system Ⓑ which approximate the fiber used in calculations in [18]. τ is obtained from Nijhof's averaging method [24].

$\beta_2^- = -1.90$ ps^2 km^{-1}	$\beta_2^+ = 6.25$ ps^2 km^{-1}
$\gamma^- = 2.30$ W^{-1} km^{-1}	$\gamma^+ = 2.30$ W^{-1} km^{-1}
$L^- = 39.4$ m	$L^+ = 11.0$ m

$\lambda_0 = 1490$ nm
$\overline{\beta}_2 = -0.121$ ps^2 km^{-1}
$\overline{\gamma} = 2.30$ W^{-1} km^{-1}
S'@1 pJ $= 1.256$ ($\tau = 334$ fs)
S'@5 pJ $= 3.435$ ($\tau = 202$ fs)
(B,S,R)@1 pJ $= (-0.055, 1.287, 0.782)$
(B,S,R)@5 pJ $= (-0.150, 3.520, 0.782)$

[1] P. Rohrmann, A. Hause, and F. Mitschke, Sci. Rep. **2**, 866 (2012).
[2] P. Rohrmann, A. Hause, and F. Mitschke, Phys. Rev. A **87**, 043834 (2013).
[3] K. S. Turitsyn and S. K. Turitsyn, Opt. Lett. **37**, 3600 (2012).
[4] C. E. Shannon, Bell Syst. Technol. J. **27**, 379 (1948); **27**, 623 (1948).
[5] L.-C. Crasovan, Y. V. Kartashov, D. Mihalache, L. Torner, Y. S. Kivshar, and V. M. Pérez-García, Phys. Rev. E **67**, 046610 (2003).

[6] R. Nath, P. Pedri, and L. Santos, Phys. Rev. A **76**, 013606 (2007).
[7] U. Al Khawaja and H. T. C. Stoof, New J. Phys. **13**, 085003 (2011).
[8] K. S. Buchanan, P. E. Roy, M. Grimsditch, F. Y. Fradin, K. Yu. Guslienko, S. D. Bader, and V. Novosad, Nat. Phys. **1**, 172 (2005).
[9] U. Al Khawaja, Phys. Rev. E **81**, 056603 (2010).
[10] Ph. Grelu, F. Belhache, F. Gutty, and J. M. Soto-Crespo, J. Opt. Soc. Am. B **20**, 863 (2003).
[11] D. Y. Tang, B. Zhao, D. Y. Shen, C. Lu, W. S. Man, and H. Y. Tam, Phys. Rev. A **68**, 013816 (2003).
[12] B. Ortaç, A. Zaviyalov, C. K. Nielsen, O. Egorov, R. Iliew, J. Limpert, F. Lederer, and A. Tünnermann, Opt. Lett. **35**, 1578 (2010).
[13] J. P. Gordon, Opt. Lett. **8**, 596 (1983).
[14] F. Mitschke and L. F. Mollenauer, Opt. Lett. **12**, 355 (1987).
[15] C. Paré and P.-A. Bélanger, Opt. Commun. **168**, 103 (1999).
[16] B.-F. Feng and B. A. Malomed, Opt. Commun. **229**, 173 (2004).
[17] A. Maruta, Y. Nonaka, and T. Inoue, Electron. Lett. **37**, 1357 (2001).
[18] A. Maruta, T. Inoue, Y. Nonaka, and Y. Yoshika, IEEE J. Sel. Top. Quantum Electron. **8**, 640 (2002).
[19] M. J. Ablowitz, T. Hirooka, and T. Inoue, J. Opt. Soc. Am. B **19**, 2876 (2002).
[20] J. D. Ania-Castanon, P. Garcia-Fernandez, and J. M. Soto-Crespo, Opt. Lett. **25**, 159 (2000).
[21] M. Stratmann, T. Pagel, and F. Mitschke, Phys. Rev. Lett. **95**, 143902 (2005).
[22] A. Hause, H. Hartwig, B. Seifert, H. Stolz, M. Böhm, and F. Mitschke, Phys. Rev. A **75**, 063836 (2007).
[23] A. Hause, H. Hartwig, M. Böhm, and F. Mitschke, Phys. Rev. A **78**, 063817 (2008).
[24] J. H. B. Nijhof, W. Forysiak, and N. J. Doran, IEEE J. Quantum Electron. **6**, 330 (2000).
[25] A. Maruta and Y. Yoshika, Eur. Phys. J. Special Topics **173**, 139 (2009).
[26] I. Gabitov, R. Indik, L. Mollenauer, M. Shkarayev, M. Stepanov, and P. M. Lushnikov, Opt. Lett. **32**, 605 (2007).
[27] I. Gabitov and S. K. Turitsyn, Opt. Lett. **21**, 327 (1996).
[28] M. Shkarayev and M. G. Stepanov, Physica D (Amsterdam) **238**, 840 (2009).
[29] A. Hause, H. Hartwig, and F. Mitschke, Phys. Rev. A **82**, 053833 (2010).
[30] S. K. Turitsyn, J. H. B. Nijhof, V. K. Mezentsev, and N. J. Doran, Opt. Lett. **24**, 1871 (1999).
[31] A. Berntson, N. J. Doran, W. Forysiak, and J. H. B. Nijhof, Opt. Lett. **23**, 900 (1998).
[32] S. K. Turitsyn, M. Fedoruk, T.-S. Yang, and W. L. Kath, IEEE J. Quantum Electron. **36**, 290 (2000).
[33] P. Y. P. Chen, P. L. Chu, and B. A. Malomed, Opt. Commun. **245**, 425 (2005).
[34] L. F. Mollenauer and J. P. Gordon, *Solitons in Optical Fibers: Fundamentals and Applications* (Academic, Burlington, MA, 2006).
[35] A. Hasegawa and M. Matsumoto, *Optical Solitons in Fibers* (Springer, Berlin, 2003).
[36] N. J. Smith, N. J. Doran, F. M. Knox, and W. Forysiak, Opt. Lett. **21**, 1981 (1996).
[37] T. I. Lakoba and D. J. Kaup, Phys. Rev. E **58**, 6728 (1998).
[38] P. Tchofo Dinda, K. Nakkeeran, and A. B. Moubissi, Opt. Commun. **187**, 427 (2001).
[39] S. Turitsyn, E. Shapiro, S. Medvedev, M. P. Fedoruk, and V. Mezentsev, C. R. Phys. **4**, 145 (2003).
[40] P. M. Lushnikov, Opt. Lett. **21**, 1535 (2001).
[41] P. M. Lushnikov, J. Opt. Soc. Am. B **21**, 1913 (2004).
[42] S. K. Turitsyn, E. W. Laedke, V. K. Mezentsev, S. L. Musher, E. G. Shapiro, T. Schäfer, and K. H. Spatschek, Opt. Commun. **151**, 117 (1998).
[43] S. K. Turitsyn, B. G. Bale, and M. P. Fedoruk, Phys. Rep. **521**, 135 (2012).
[44] M. Stratmann and F. Mitschke, Phys. Rev. E **72**, 066616 (2005).
[45] J. M. Soto-Crespo, N. Akhmediev, Ph. Grelu, and F. Belhache, Opt. Lett. **28**, 1757 (2003).